

Improved signal detection algorithms for unevenly sampled data. Six signals in the radial velocity data for GJ876

J.S. Jenkins^{1*}, N. Becerra Yoma², P. Rojo¹, R. Mahu², J. Wuth²

¹*Departamento de Astronomía, Universidad de Chile, Camino el Observatorio 1515, Las Condes, Santiago, Chile, Casilla 36-D*

²*Dept. of Electrical Engineering, Universidad de Chile, Av. Tupper 2007, PO Box 412-3, Santiago, Chile*

Submitted January 2011

ABSTRACT

The hunt for Earth analogue planets orbiting Sun-like stars has forced the introduction of novel methods to detect signals at, or below, the level of the intrinsic noise of the observations. We present a new global periodogram method that returns more information than the classic Lomb-Scargle periodogram method for radial velocity signal detection. Our method uses the Minimum Mean Squared Error as a framework to determine the optimal number of genuine signals present in a radial velocity timeseries using a global search algorithm, meaning we can discard noise spikes from the data before follow-up analysis. This method also allows us to determine the phase and amplitude of the signals we detect, meaning we can track these quantities as a function of time to test if the signals are stationary or non-stationary. We apply our method to the radial velocity data for GJ876 as a test system to highlight how the phase information can be used to select against non-stationary sources of detected signals in radial velocity data, such as rotational modulation of star spots. Analysis of this system yields two new statistically significant signals in the combined Keck and HARPS velocities with periods of 10 and 15 days. Although a planet with a period of 15 days would relate to a Laplace resonant chain configuration with three of the other planets (8:4:2:1), we stress that follow-up dynamical analyses are needed to test the reliability of such a six planet system.

Key words:

stars: planetary systems, stars:individual-GJ876, methods: data analysis, stars:
activity

1 INTRODUCTION

The discovery and characterisation of low-mass rocky planets is moving at a fast pace, now that technology has reached the limit necessary to discover these elusive objects. Along with the technological advances, a number of stars have been monitored with long enough time baselines to gain the necessary clutch of data points that allows low-amplitude signals to be announced with a high level of statistical significance.

Teams discovering these planetary systems generally use the classic method of applying a Lomb-Scargle periodogram (LSP) algorithm to their data, which looks for the presence of sine and cosine functions buried in any discretely sampled timeseries (Scargle 1982). This method has been very successful in finding low-amplitude signals that betray the presence of small planets (e.g. Mayor et al. 2009; Vogt et al. 2010), however it has recently been shown to be an inefficient way to detect such signals (Tuomi & Jenkins 2012).

At this point it is worth introducing a short explanation of where in the procedure of planet detection the LSP fits in. Once the observations of a given target star have been converted into Doppler velocity points, the timeseries is fed to the LSP. The periodogram performs a Fourier-like analysis of the data, and the observer then searches for the most powerful frequencies output by the algorithm. The observer can then move to the next step, which is characterisation of any frequency found by the algorithm, proving if this frequency is a genuine Doppler shift or not. Therefore, the LSP algorithm plays a fundamental role in planet detection, since if the power of any Doppler frequency is not highlighted, the planetary signal will remain hidden.

Another method that has recently been employed to search for low-amplitude signals in radial velocity data is through Bayesian analysis (Tuomi 2012; Tuomi & Jenkins 2012), and this has given rise to a number of new, and low-mass, planetary systems (e.g. Anglada-Escudé et al. 2012; Tuomi et al. 2013; Jenkins et al. 2013). Although, Bayesian analysis seems to detect low-amplitude signals more efficiently than application of the LSP method, it is not as easily applicable as the LSP method and is less intuitive, so is not widely used in the exoplanet community.

* E-mail: jjenkins@das.uchile.cl

With this in mind, we have begun a program to move beyond the LSP, such that we can detect low-amplitude signals with greater efficiency, and with greater certainty than is currently possible. In § 2 and § 3 we describe the LSP methodology, and our first step along the path to implementing better detection methods that surpass the LSP algorithm. In § 4 we describe the comparison tests we did with the LSP, and highlight the areas where our algorithm can provide greater benefits. In § 5 we apply our algorithm to the radial velocity data set from Keck and HARPS for the star GJ876, which is known to host a dynamically stable system of at least four planets, three of which are in a Laplace resonance. Finally, we summarise our code and results in § 6.

2 LOMB-SCARGLE PERIODOGRAM

Classically in the exoplanet field, Keplerian orbits have been detected in radial velocity data by application of the LSP (Scargle 1982). The LSP was developed as a tool to statistically evaluate the level of significance of any detected periodic signal in unevenly sampled data by translating the data into the Fourier domain and searching for sine and cosine patterns that repeat. Sine and cosine functions that are stable and well sampled manifest as strong peaks in the power spectrum of such data, and an observer can then select the strong peaks that pass some significance threshold, and study the velocities for the presence of planets. The complications arise from the spectral window function and the additive noise in the data.

Although the LSP has been an extremely successful tool in astrophysics, the method has some drawbacks, which we will explain here in the context of the search for exoplanets. The LSP base algorithm is shown in Eqⁿ 1 and one can see that the method performs a Fourier transform of the data and then searches for periodic sinusoidal frequencies using a sine and cosine based method:

$$P_X(\omega) = \frac{1}{2} \left\{ \frac{\left[\sum_j X_j \cos \omega(t_j - \tau) \right]^2}{\sum_j \cos^2 \omega(t_j - \tau)} + \frac{\left[\sum_j X_j \sin \omega(t_j - \tau) \right]^2}{\sum_j \sin^2 \omega(t_j - \tau)} \right\} \quad (1)$$

where P_X is the periodogram powers as a function of frequency, ω is the sinusoidal frequencies, t_j are the timestamps of the observations, and τ is defined as follows:

$$\tan(2\omega\tau) = \frac{\left(\sum_j \sin 2\omega t_j \right)}{\left(\sum_j \cos 2\omega t_j \right)} \quad (2)$$

The power of this algorithm comes from the fact that when the data (X) contains a sinusoidal component that has a characteristic frequency ω_0 , then around $\omega = \omega_0$, this frequency is in phase with the introduced sinusoidal factors in the Fourier domain, and the signal strength is increased. The signal then appears as a strong peak in the power domain when compared to other peaks across the full frequency window that has been sampled.

One issue with this method is that the sine and cosine functions applied in the signal search are not strictly orthogonal for unevenly sampled data, meaning that the power spectral points, P_X , are not independent variables, which means they are correlated. Scargle (1982) discussed this issue and was able to show that this dependence can be limited by construction of a well chosen frequency grid to sample the Fourier domain. However, when applied to low S/N data, such as low-amplitude signals in radial velocity data produced by orbiting low-mass planets, this inter-dependency in the power spectrum complicates the signal detections, particularly for a superposition of low-amplitude signals arising from multiple low-mass planets.

Another issue in the search for planetary orbits from radial velocity data is that there are a high fraction of reported planets that are not in circular orbits that are well described by single sine and cosine functions, but rather require a more complex Keplerian function to describe them. O’Toole et al. (2009) introduced a new method to search for frequencies in radial velocity data that directly employs a Keplerian search algorithm, following a number of the descriptions in Cumming (2004), that appears to be significantly better at detecting signals from planets on highly eccentric orbits.

Additionally, in the LSP the noise properties for the data X are assumed to be white when computing the statistical significance of each sampled frequency point. For precision radial velocity work, it is now known that the velocities themselves can exhibit significant correlations (see Baluev 2013; Tuomi & Jenkins 2012), correlations that should be accounted for. Therefore, in the strictest sense, analytical FAPs calculated using the equations laid out in Scargle (1982) are incorrect, given the underlying assumption of Gaussian distributed noise. Therefore, the presence of correlated noise increases the difficulty of detecting signals using an approach that does not consider that noise in any way.

More practically, given the method of signal detection in exoplanetary science, the normal multi-planet detection methods introduce problems. The standard approach is as follows:

- (i) Apply the LSP to the radial velocities

- (ii) Locate the strongest and significant signal at a given frequency (orbital period)
- (iii) Fit a Keplerian function to the velocities around that period and subtract off to get the residuals
- (iv) Re-apply the LSP to the residuals to search for additional signals in the data
- (v) Repeat until the white noise floor is reached or there are no significant peaks remaining

This procedure is not optimal for detecting low-amplitude signals buried in the noise of radial velocity timeseries data sets because once a signal has been detected and fit out, a search for additional signals in the residuals will depend on the original model that was subtracted off, since generally these signals are not orthogonal. New approaches have been introduced to try to circumvent this issue, such as applying Bayesian inference, mentioned above, or recursive periodogram methods (Baluev 2013; Anglada-Escudé & Tuomi 2012).

Finally, the LSP by definition is a method that works by measuring the harmonic content of any signals present in the power spectrum of a data set, which means that there is no information provided by the algorithm on the amplitude or phase of the signal found in the data. This means that any signal detected by the LSP that is then searched for by using a least-squares Keplerian fitting procedure in the velocities, is not guaranteed to be the same signal. In real terms it is highly likely that the signal fit is the same signal, but without additional information from the LSP, it is difficult, if not impossible, to prove this. In addition, the amplitude and phase of a signal contains vital information, since they can be used to show that any signal detected is a true *stationary* Doppler signal, or is a quasi-stationary signal that could arise from time-dependent phenomena on the star such as spot rotation (e.g. Dawson & Fabrycky 2010).

Given the limits of the LSP method for low-amplitude signal detection in unevenly sampled data mentioned above, we have devised a method based around the minimum mean square error (MMSE) that can allow the period, amplitude, phase, and number of components that best describes the data set, to be found directly from the search algorithm itself. The following section is devoted to explaining our methodology. We note that Zechmeister & Kürster (2009) introduced the Generalised Lomb Scargle Periodogram method that handles better more eccentric Keplerian orbits. However, our MMSE method has specifically been designed to determine the number of real components in a data set in a global fashion, in order to aid in the detection of the emerging population of low-mass and circular multi-planet systems. However, it is fairly trivial to add an extra offset component

to the following MMSE algorithm that will perform the same function as the Generalised LSP.

3 MINIMUM MEAN SQUARE ERROR

Our MMSE method utilises five steps sequentially in order to estimate the most significant components in a sequence of samples generated with non-uniform sampling. Firstly, a Fourier-like analysis is run on the data, using the MMSE, and the components with the lowest square error are selected from the resultant MMSE series. Secondly, the local neighbourhoods of those components are selected for scrutiny. Next, the MMSE is then recomputed for all possible combinations of components and their neighbours, selected in the previous steps. Finally, the combination with the lowest MMSE is chosen as the most significant sinusoidal components of the given data sets.

We introduce our analysis method using the MMSE in the following manner. Given a set of data, such as radial velocity measurements that contain any number of frequencies that we will assign $x(i)$, where $1 \leq i \leq I$ and I is the length of the data set, we can estimate the number of sinusoidal components N_C , and the set $S = \{C_1, C_2, \dots, C_i, \dots, C_{N_C}\}$ where C_i corresponds to the i -th sinusoidal component, by formulating the set of frequencies like Eqⁿ 3:

$$S = \{(\omega_1, a_1, \phi_1), \dots, (\omega_i, a_i, \phi_i), \dots, (\omega_{N_C}, a_{N_C}, \phi_{N_C})\} \quad (3)$$

where (ω_i, a_i, ϕ_i) corresponds to the frequency, amplitude, and phase of the i -th component in C_i . Therefore, by application of the MMSE method, the problem can be formulated as finding the set $S = \{(\omega_i, a_i, \phi_i)\}_{i=1}^{N_C}$ that satisfies the following minimisation:

$$S = \arg \min_{\omega_i, a_i, \phi_i} \left\{ \sum_{t=1}^T \left(X(t) - \sum_{i=1}^{N_C} a_i \cos(\omega_i t + \phi_i) \right)^2 \right\} \quad (4)$$

where the sinusoidal components present in $X(t)$ are given by the set of triplets with the minimum square error, and N_C corresponds to the number of triplets present in the analysis.

Solving Eq. 4 requires an exhaustive search over N_C , ω , a , and ϕ . Even if N_C were known a priori, the number of possible combinations of ω , a , and ϕ are beyond computational capacity. Let the target frequency bandwidth, the amplitude, and the phase be divided into K_ω , K_a , and K_ϕ levels respectively, then the number of possibilities for taking N_C triplets (ω, a, ϕ) simultaneously is $(K_\omega \cdot K_a \cdot K_\phi)^{N_C}$. Since all possible values of ω , a , and ϕ have

to be explored, the program is unfeasible from the point of view of computational load. For instance, if we consider high precision in frequency ($K_\omega \approx 10^3$) and moderate precision in amplitude and phase ($K_a \approx 10^2, K_\phi \approx 10^2$), the number of possible combinations of ω , a , and ϕ grow rapidly, since for $N_C = 7$, and considering that each combination can be evaluated in one CPU instruction, 10^{49} instructions are necessary, which would require more than 10^{39} seconds or approximately 3×10^{31} years on a 10 GHz processor, clearly not a calculation that can be done in any reasonable time frame. As an alternative, a MMSE based method is proposed since it can be easily implemented in multi-core computing, reducing the processing time drastically.

Step 1: The first step is to perform a MMSE based Fourier analysis, where the target frequency bandwidth is divided into K_ω levels. Each level ω_k is represented by

$$\omega_k = \frac{\pi * k}{K_\omega}, \quad \text{where } 1 \leq k \leq K_\omega \quad (5)$$

For each ω_k an optimal amplitude a_{ω_k} and phase ϕ_{ω_k} are computed according to the following equation:

$$(a_{\omega_k}, \phi_{\omega_k}) = \underset{a, \phi}{\operatorname{argmin}} \left\{ \sum_{t=1}^T (X(t) - a \cos(\omega t + \phi))^2 \right\} \quad (6)$$

By application of Eqⁿ 6, a set S_P of components is obtained as shown in Eqⁿ 7

$$S_P = \{(\omega_k, a_{\omega_k}, \phi_{\omega_k})\}_{k=1}^{K_\omega} \quad (7)$$

This set corresponds to the new periodogram of the data.

Step 2: Now one must select the N components that show the lowest MMSE, either by visual inspection or by automatically selecting all MMSE values below a threshold level selected at the discretion of the user, or based on some noise threshold criteria (e.g. Kuschnig et al. 1997). From the set S_P obtained in the previous step, a subset $S_{min} = \{(\omega_i, a_{\omega_i}, \phi_{\omega_i})\}$ is built with the N components that show the lowest MMSE or the highest amplitudes.

Step 3: For each component C_i associated with the triplet $(\omega_i, a_{\omega_i}, \phi_{\omega_i})$ in S_{min} , a neighbourhood V_i is defined, according to Eqⁿ 8

$$V_i = \{(\omega, a_{\omega}, \phi_{\omega}) \in S_P / \omega \in [\omega_i - \delta, \omega_i + \delta]\} \quad (8)$$

where δ is defined as the number of elements of V_i that are lower than N_{\max} , and N_{\max} defines the maximum number of elements of any neighbourhood. Therefore, δ is set to some value to incorporate all the significant S_P peaks. As a result, each component $C_i(\omega_i, a_{\omega_i}, \phi_{\omega_i})$ provides M_{C_i} candidates, where M_{C_i} is given by the cardinality of V_i .

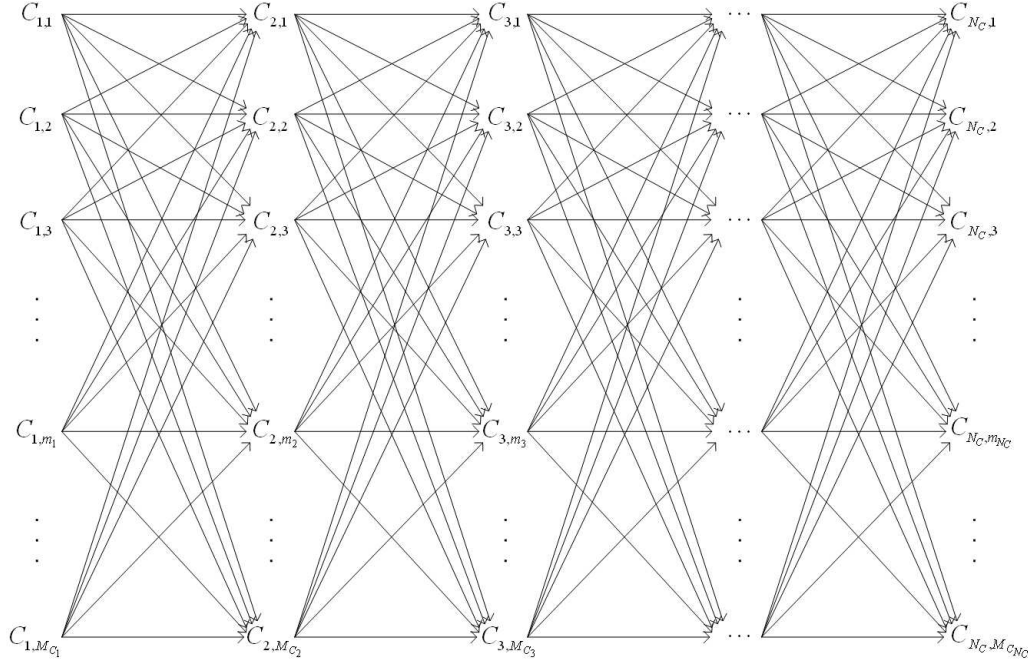


Figure 1. An example trellis diagram, illustrating all the possible combinations of components and their local neighbourhoods.

We note that an alternative to the neighbourhood defined around each component C_i , the trellis analysis can be performed by taking into consideration the frequency of C_i only. In this case, another neighbourhood can be defined by considering sets of amplitudes and phases to assess the validity of C_i as a true component of the data set.

Step 4: The MMSE is computed for all the possible combinations of N_C components, where N_C is lower than or equal to N . A trellis is generated with all the candidates per component (see Fig. 1). For each $N_C < N$, let $A^j = \{C_1^j, C_2^j, \dots, C_{N_C}^j\}$ be a set with one of the combinations of N_C components from N , where $1 < j < \frac{N!}{N_C!(N-N_C)!}$ and C_i^j corresponds to the i th component in the j th combination. The corresponding set of neighbourhoods is $V_{A^j} = \{V_1^j, V_2^j, \dots, V_{N_C}^j\}$ where V_i^j denotes the neighbourhood of components C_i^j . For each A^j , the set of N_C triplets $(\hat{\omega}_1^j, \hat{a}_1^j, \hat{\phi}_1^j), \dots, (\hat{\omega}_{N_C}^j, \hat{a}_{N_C}^j, \hat{\phi}_{N_C}^j)$ is found whereby the lowest MMSE is obtained according to Eqⁿ 9.

$$(\hat{\omega}_1^j, \hat{a}_1^j, \hat{\phi}_1^j), \dots, (\hat{\omega}_{N_C}^j, \hat{a}_{N_C}^j, \hat{\phi}_{N_C}^j) = \arg \min_{(\omega_i^j, a_i^j, \phi_i^j) 1 \leq i \leq N_C} \sum_{t=1}^T \left(X(t) - \sum_{i=1}^{N_C} a_i^j \cos(\omega_i^j t + \phi_i^j) \right)^2 \quad (9)$$

where $(\hat{\omega}_i^j, \hat{a}_i^j, \hat{\phi}_i^j) \in V_i^j$, $1 \leq i \leq N_C$ and in this way, an optimal set of N_C triplets is obtained for each N_C .

Step 5: Finally, one must choose the N_C that minimises the MMSE. To do this we let $S = \{(\hat{\omega}_1, \hat{a}_1, \hat{\phi}_1), \dots, (\hat{\omega}_{N_C}, \hat{a}_{N_C}, \hat{\phi}_{N_C})\}$ be the set with the lowest MMSE obtained in the

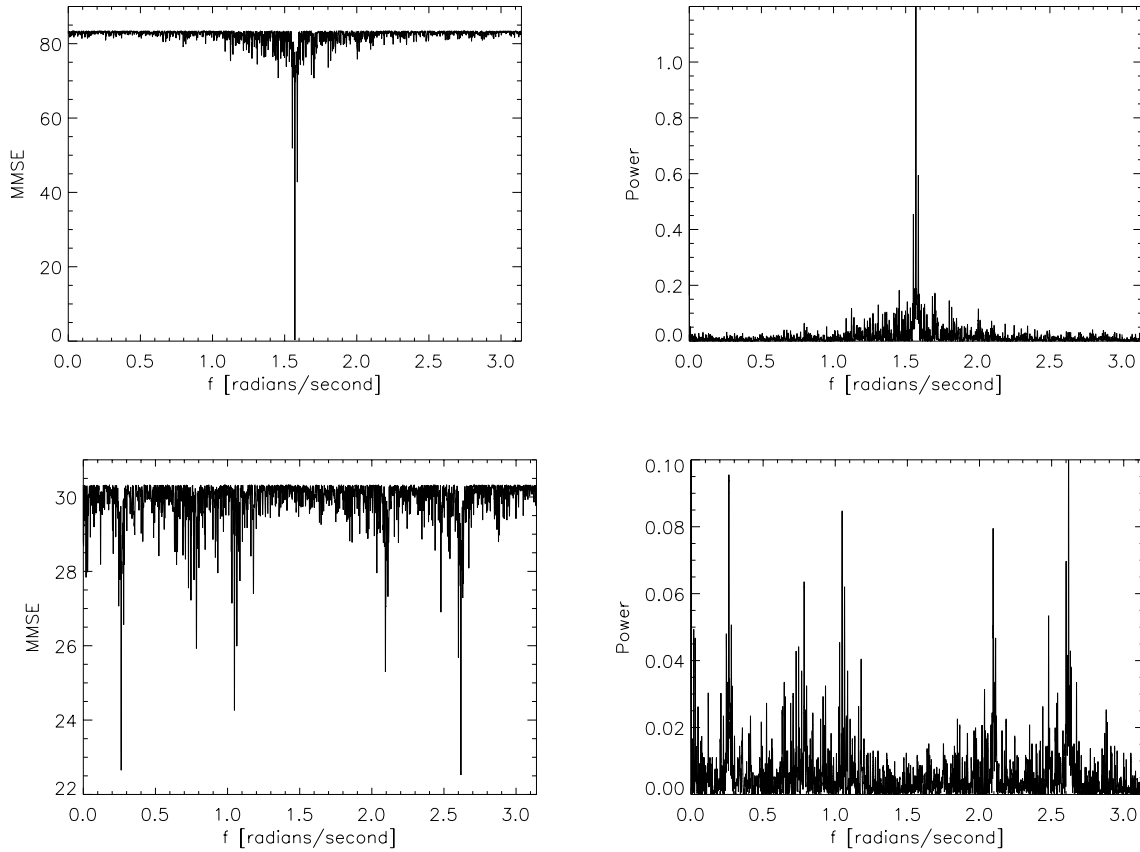


Figure 2. The left column corresponds to the MMSE periodograms, where the detection of a simulated pure signal (top) and a signal with harmonics included (bottom) are shown. The right column shows the same signals detected with the LSP.

previous step. The most important sinusoidal components present in the data set are given by the N_C triplets in S .

4 FUNCTIONALITY TESTS

In order to test the reliability of the algorithm we describe above, we ran two tests on simulated data where 1) we simulate a pure signal and 2) we simulate superposition of five signals without harmonics present. We also run the same tests on the LSP and compare the results from both.

4.1 Pure Signal

In the top panel of Fig. 2 we compare the MMSE values against the LSP powers as a function of frequency for a pure signal implanted in a simulated radial velocity timeseries with uneven sampling. The signal was generated simply as $a * \cos(\omega t + \phi)$, where $a=1.0998$, $\omega = \pi/2$, and $\phi=2$. We note that with even sampling the signal is significantly stronger and the noise

spikes are heavily suppressed as they primarily arise due to interference from the window function from unevenly sampled data.

In both analyses we recover the signal with low false alarm probability (FAP) at a frequency of 0.25 Hz, or $\pi/2$ radians per second (1.5708 rads/sec), as shown in the top plots in Fig. 2. The FAP's were calculated following a bootstrap method where we scrambled the velocities with replacement, computing the periodograms each time and comparing the strength of the strongest frequency to the observed frequency, recording the number of times this frequency was stronger than the observed frequency power. This allowed us to calculate the probability that our observed strongest frequency could arise by chance given the data. The FAP's we calculated are both significantly $<10^{-4}$ and it can be seen that the noise falls off in a Lorentzian fashion when moving progressively further away from the central strong peak.

4.2 Tests without Harmonics

The lower panels in Fig. 2 show a similar simulated data set to the top panels, except five signals at various frequencies have been introduced without signal harmonics. The signals were introduced as follows, $a_1 * \cos(\omega_1 t + \phi_1) + a_2 * \cos(\omega_2 t + \phi_2) + \dots + a_5 * \cos(\omega_5 t + \phi_5)$, with parameter values of $a_1 = a_2 = \dots = a_5 = 0.3083$, $\phi_1 = \phi_2 = \dots = \phi_5 = 2$, and ω_i values, where $1 \leq i \leq 5$, of $\pi/12, 3\pi/12, 4\pi/12, 8\pi/12$, and $10\pi/12$ radians, respectively.

It can be seen that the strength of these periodogram peaks are dramatically reduced, in comparison to the strength of the single pure peak found in the top panels. In the LSP on the right, we see the five strong peaks across the frequency band of interest (0.0-0.5 Hz). There are also secondary signals, not as strong as these five, but with significant power to decrease the significance of signal detection. The introduced signals were recovered as the strongest peaks in this data, however after subtracting each one away, a process that is common in the exoplanet detection field, again the FAP's were extremely low, even in the presence of the other peaks.

The MMSE periodogram is very similar to the LSP, as expected. The same patterns arise in the analysis, similar frequency peaks and surrounding noise peaks, and the FAP's of the signals are also similar to the LSP probabilities. Therefore, this shows that, to first-order, the MMSE is as powerful as the LSP for detecting multiple signals in a radial velocity

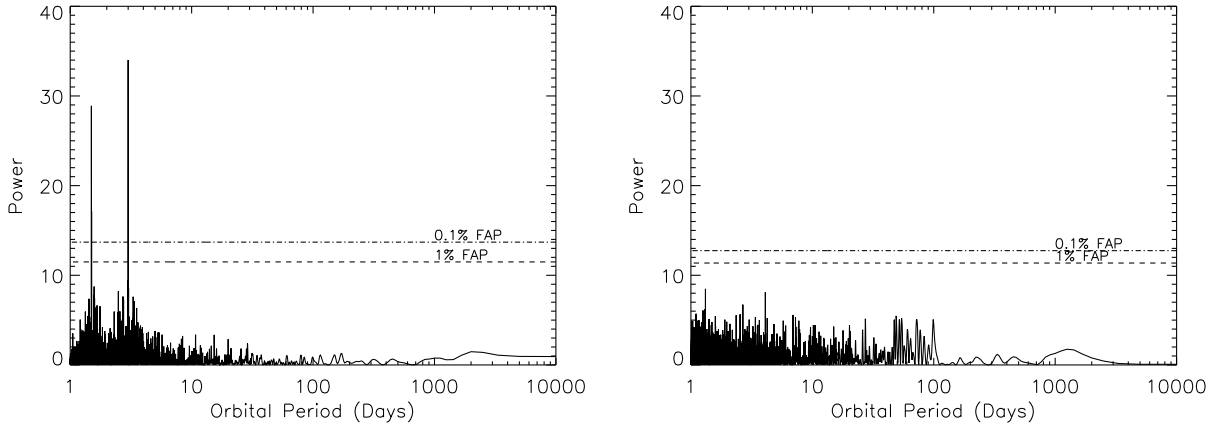


Figure 3. Periodograms for a simulated system of two planets with periods of 3 days and 100 days and circular orbits. The left panel is the raw periodogram and right panel is the periodogram of the residuals after subtraction of the best fit orbit for the inner planet. The FAP's for 1 and 0.1% are shown for reference.

timeseries, and the presence of additional signals in a data set does not adversely affect the MMSE method any more than it does the LSP.

4.3 Component Test

Above we have shown that the MMSE is as effective at detecting circular signals as the LSP, even though the MMSE also returns more information about the signals that have been tested. We note that methods such as prewhitening can also return the period, amplitude, and phase of a signal, and prewhitening has been used to constrain the mass of Corot-7b (Queloz et al. 2009; Hatzes et al. 2010) and to shed some doubt on the nature of the planet candidate orbiting α Centauri B (Hatzes 2013). There are also packages available to perform this type of analysis, Period04 for example (Lenz & Breger 2004).

As mentioned earlier, the downside to using methods such as prewhitening is that they are gradient based approaches that start by searching for one signal only, subtracting that signal out of the timeseries, and then searching the residuals all over again by treating the residuals as an independent timeseries from the original observed data, and then repeating this process until the noise floor is reached. Our MMSE method on the other hand is a global approach that searches for all signals in a timeseries at the same time. The value in this approach, at the cost of computing time, is that we make no assumption that the original timeseries only contains one signal, which is implicit in a gradient based approach, and hence we do not lose any of the power in secondary signals that is lost when subtracting out the primary frequency detected by the LSP/prewhitening approaches.

As a test we simulated a system of two planets with orbital periods of 3 and 100 days, such that the high frequency signal was clearly detected in the original data but the lower

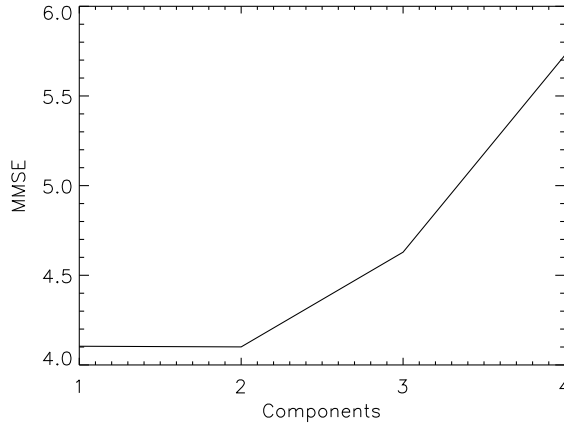


Figure 4. Number of components detected by our trellis MMSE signal search in the two planet simulation. The solid curve is minimised at two, centered on both signals in the simulated data set.

frequency peak was not apparent, even after subtraction of the higher frequency signal (see Fig. 3). Following our MMSE approach, we then selected a number of the deepest spikes in the periodogram and performed the trellis component search part of our method. The search was able to determine that the data contained two, and only two, components, returning their periods, amplitudes, and phases. The minimum of the curve in Fig. 4 represents the detected number of signals in the data set. This test shows that a global approach like this can be more powerful than a gradient based approach, particularly for detecting the emerging population of multi-planet low-mass systems.

5 APPLICATION TO THE GJ876 DOPPLER VELOCITIES

GJ876 is a M-dwarf star that hosts a system of at least four planets, two of these planets are gas giants that have been found to be orbiting in a Laplace Resonance with one of the smaller planets in the system (Rivera et al. 2010). Although, we expect that the resonance acts to rapidly alter the orbital elements of these planets, the two gas giants exert large velocity variations on the star large enough that both planets are easily detectable in the first and second halves of the data independently, and the signal is much larger than any variations in the elements we expect. This represents a good test data set for our method as there are enough data points to detect multiple signals and the data sets come from two independent instruments and analysis methods.

5.1 Reanalysis of Planetary System

The planetary system around GJ876 has an important place in the history of exoplanet science, since it was the first planetary system shown to have planets in some resonant

configuration (Marcy et al. 2001). Resonances had been witnessed in the moons of Jupiter and various asteroid and planetary configurations in our Solar System. It has been hypothesised that a previous 1:2 resonance of Jupiter and Saturn was the reason for the late heavy bombardment and the final positions of the outer giant planets (Tsiganis et al. 2005; Morbidelli et al. 2005). However, the two gas giants orbiting GJ876 were the first exoplanets actually found to be in a resonant configuration, indicating that dynamical interactions of planetary bodies are indeed an important ingredient in the formation and evolution of planetary systems.

Currently four planets are known to orbit this star, with orbital periods of 1.94, 30.09, 61.12, and 124.26 days (Delfosse et al. 1998; Marcy et al. 2001; Rivera et al. 2005; Rivera et al. 2010), but there exists the exciting potential for more. Correia et al. (2010) performed many dynamical simulations that suggest a planet with an orbital period of around 15 days could stably exist in a larger chain resonance, however they claimed that the radial velocity data did not support such a planet, and therefore if there is a planet with an orbital period of 15 days it can not have a mass any larger than around $2 M_{\oplus}$. Such a result motivates the search for additional signals in the GJ876 velocities.

In Fig. 5 we show our MMSE analysis for GJ876 data from Keck (Rivera et al. 2010) and HARPS (Bonfils et al. 2013), where the HARPS data have been processed using the TERRA pipeline (Anglada-Escudé & Butler 2012), and in addition to the currently known signals originating from four planets, we highlight two new planet-like signals in the data. In the top and second top panels we can see the strongest two signals, originating from the two gas giants known to be in resonance, with periods of around 61 and 30 days respectively. The first of the new signals (planets?) has an orbital period of 15 days (third panel down in the figure), placing it in the region of stability found by Correia et al., but the mass of this planet would be $0.1 M_J$, much larger than that speculated by Correia et al. or Rivera et al.. Indeed, it was not possible to reach the χ^2 values or rms values quoted in these works without including this signal in the data by following the standard radial velocity planet detection procedure of analysing a periodogram, selecting the strongest statistically significant signal, fitting that signal with a Keplerian, subtracting off that signal, and then reanalysing the residuals to hunt for addition frequencies.

The omission of discussion of this signal from previous works is puzzling, since the signal has a semi-amplitude of 20 ms^{-1} . Since this signal is circular, and if this signal were to arise from a genuine gas giant planet found to be in an island of stability due to the Laplace

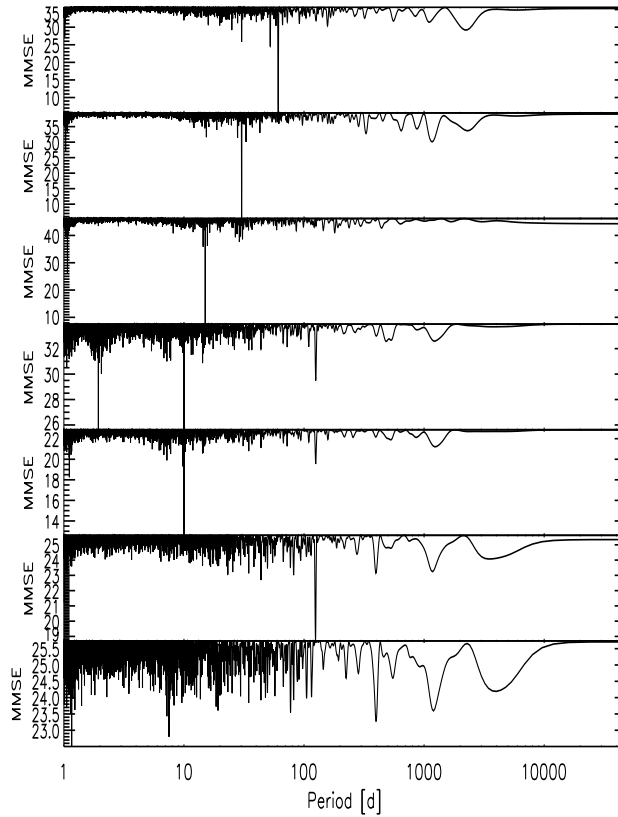


Figure 5. MMSE periodograms for the signals detected in the GJ876 radial velocities. From top to bottom we show the raw velocities, followed by the MMSE periodograms after subtracting each signal sequentially (61, 30, 15, 1.9, 10, and 124 days, respectively).

resonance, it would also indicate that the other planetary orbits could be more circular than previously thought. In fact, we found the best fit by fixing all the orbits in the system to zero throughout the process. The inclusion of this signal does not decrease the amplitudes of the previous planetary signals, meaning the masses previously found remain, only the orbits are circularised for some of them. Anglada-Escudé et al. (2010) and Wittenmyer et al. (2012) have shown that resonant planets can be mistaken for less planets in a system but with higher orbital eccentricities.

Even though the MMSE spike for this 15 day signal is very significant, having a FAP lower than 10^{-4} , we still must ensure that it does not originate from any interference by the window function, especially since it is near half the lunar cycle period. To test this we generated a fake system including only the first two planets, GJ876*b* and *c*, which have the strongest signals prior to the 15 day signal, fit them out and then see what remains in the data. We keep the observed timestamps and uncertainties in this process. We found that no significant signal at any frequency is present in the data after fitting out the first two

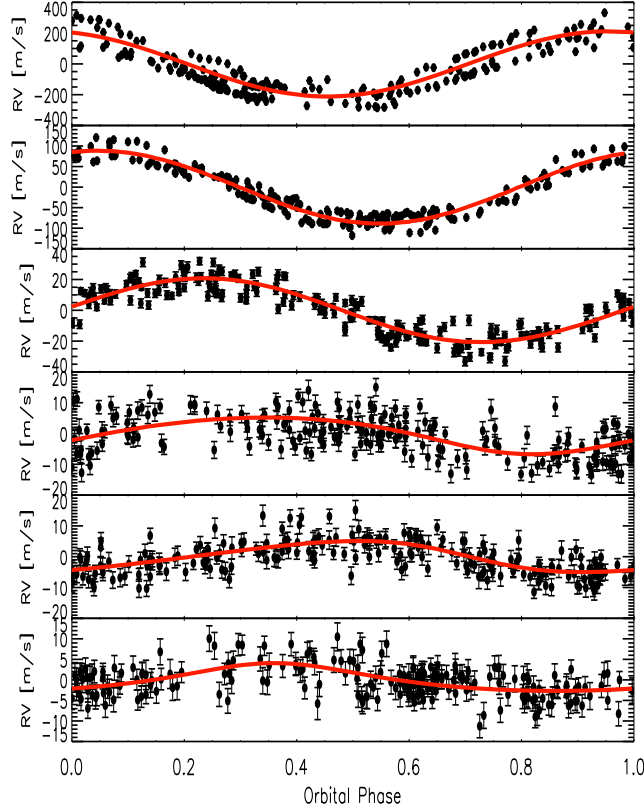


Figure 6. Phased radial velocity curves for all six signals detected in the combined Keck and HARPS-TERRA Doppler velocities. From top to bottom we show signals with periods of 61, 30, 15, 1.92, 10, and 124 days, respectively. The red curve shows the best fit Keplerian solutions we find for each of these signals.

signals. This is also the case if we inject all four of the previously known signals and rerun this experiment. This tells us that the 15 day signal is present in the observed data set.

After considering the 15 day signal, the next strongest peak is the 1.93 day planet that was previously known (fourth panel down in Fig 5), found to be significant in our combined data set. However, after considering this planetary orbit, the next signal that emerges from the data is not the outer planet beyond 120 days, but a 10 day signal that we show in fifth panel of the figure. We note that this signal was almost as significant as the 1.93 day signal after removal of the 15 day signal from the data. This signal again has a FAP of less than 10^{-4} , meaning it is statistically significant in the data. This signal has a semi-amplitude of 4.97 ms^{-1} , and if it was from an additional orbiting planet in this system, it would relate to a planet with a minimum mass of $0.02 M_J$.

Finally in the sixth panel of Fig 5 we can see the signal from the outer planet with a period of 124.7 days. This signal is well above the level of significance threshold to claim the existence of a signal, confirming this planet does still fit within the configuration we have discovered in the current data. If we make the bold assumption that all of these signals

are from orbiting planets in the GJ876 system, then the system contains a likely 8:4:2:1 Laplace resonance between four planets, three of which are gas giants orbiting this M-dwarf, something that is known to be rare, and two low-mass planets interior to the resonance, all of which have close to circular orbits. However, given the total mass that the three largest planets would maintain (periods of 61, 30, and 15 days respectively), it is necessary to perform further dynamical simulations to test if such a system could be stable over the long term. The previous works that do find islands of stability around 15 days do give us hope that at least one of these two signals originates from a planetary orbit, and if it is at 15 days, it is highly likely that we have found a new Laplace resonant chain. The phase folded velocity curves for all six signals we have detected are shown in Fig. 6.

A non-planetary origin might be expected for the 15 day and 10 day signals since both the Correia et al. (2010) and Rivera et al. (2010) analyses failed to spot them when applying a Newtonian integration analysis that considers the dynamical interactions between the planets. Although both these works suggested there are islands of stability around 15 days, Gerlach & Haghighipour (2012) suggest that these islands are likely not long-term stable given the planetary system configuration suggested by these works. However, they show that planets on orbits exterior to the currently known outer planet in this system could exist in long-term stable orbits. We note that after all the previous signals have been considered we see two emerging spikes in the MMSE, one with a period of around 400 days and the other with a period of 1250 days. These could be the first indications of additional longer-period planets in the GJ876 system, motivating continued observation of this highly prized and nearby planetary system.

There is the possibility that these signals are due to rotationally modulated spots on the stellar surface manifesting as an apparent velocity shift due to deformations of the spectral lines used to calculate the Doppler velocities. Such activity induced signals can be measured and tracked using specific indicators like the Calcium HK chromospheric lines (Jenkins et al. 2011), or possibly even corrected for using measurements of the line bisectors (see Jenkins et al. 2009). In the case of GJ876, both Rivera et al. (2005) and Rivera et al. (2010) show that the rotation period for this star is around 90-100 days, using photometry and CaII HK measurements respectively. Therefore, it is unlikely that the new strong frequencies we see in the combined Keck and HARPS data are due rotational modulation of star spots, since we would be detecting harmonic frequencies beyond the 3rd-order. Finally, the Keck and HARPS-TERRA radial velocities are shown in Table 1, the final system

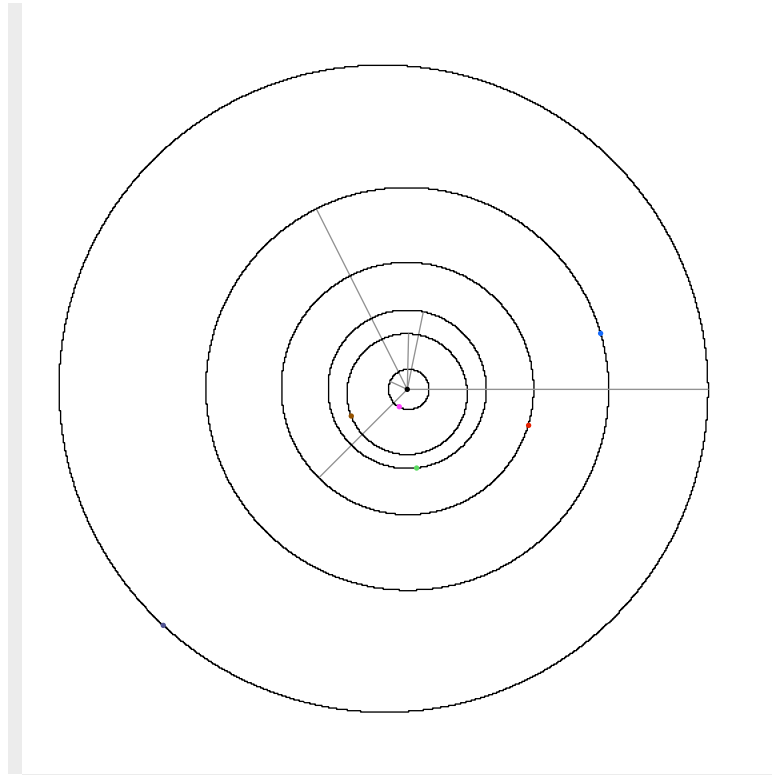


Figure 7. Orbital configuration of the possible planetary system orbiting GJ876.

configuration is shown in Fig. 7 (output from the Systemic Console; Meschiari et al. 2009), assuming all originate from planetary orbits, and a list of the signal parameters are shown in Table 2. All uncertainties were calculated using the Markov Chain Monte Carlo routines within the Systemic Console.

5.2 Amplitude, Phase, and Number of Components

In the previous sections we have described our procedure for signal detection in unevenly sampled timeseries that contains stationary and repeating signals, such as a radial velocity timeseries containing Doppler signals induced by planets orbiting a star. We have also shown that the proposed MMSE method works at least as well as the classical LSP method of signal detection, and when applied to signal rich data like that for GJ876, it has no problem in detecting multiple signals in the data. However, now we will show the power of the MMSE over the LSP method, in particular focusing on the additional information provided by our method.

Looking back at Eqⁿ 4, we see that our MMSE method does not only focus on properties inherent in the spherical harmonics, or orthogonal sine and cosine functions, but it also minimises properties of the signal that are present in the unevenly sampled data set.

In particular, this method constrains the amplitude (a), the phase (ϕ), and also the number of components that best describe the timeseries in the presence of noise (N_C). Such information can be invaluable in timeseries analysis. For example, when trying to confirm the nature of low-amplitude signals in a radial velocity timeseries one can assess the phase and amplitude as a function of time to ensure that these properties of the signal are more or less constant, which would be expected from a quasi-stationary source like stellar activity (see Dawson & Fabrycky 2010). The number of components that best describe the data can also be used in this sense to estimate the upper-limit of planetary signals one should search for in the data and anything else can be considered as noise.

5.3 Phase Test for GJ876*b* and *c*

Lets take the case of the confirmed gas giant planets orbiting GJ876. The hypothesis is that if the two signals are more or less stationary, as they should be if they originate from the Doppler effect induced by the gravitational tug of these planets, then the phase offset ($O = \phi_1 - \phi_2$) between the two signals, or indeed the phase of each signal independently, should also be essentially stationary as a function of time, i.e. both signals conserve their phase across the baseline of the timeseries. Therefore, with enough data across a time baseline long enough to confidently sample a double planet signal, we can measure the phase of both signals in the first half of the data set, do the same for the second half of the data set, and ensure that they are equal (i.e. $O_1 - O_2 = 0$), within some tolerance level, essentially ensuring that the phase does not vary with time. A similar analysis can be performed on the amplitude of these signals, or of course, the frequencies aswell. We have shown previously the significance of the signals for planets *b* and *c* orbiting GJ876 are very strong and given our current data we can clearly detect both of these signals in the first and second halves of the velocity timeseries independently.

First of all, we ran the analysis as we did before on this data using the procedural steps we outlined in § 3. For clarity we again show the MMSE periodogram in the top panel of Fig. 8 for the full radial velocity data set, and we found both of the planetary frequency spikes to be in the first three strongest spikes, as expected. We then selected a few of the deepest spikes and ran the component analysis, as we did before on the simulated data in § 4. Since the peaks we selected contain the two gas giant planetary signals, the component search returns a value of two, possibly three, components in the curves (lower panel in

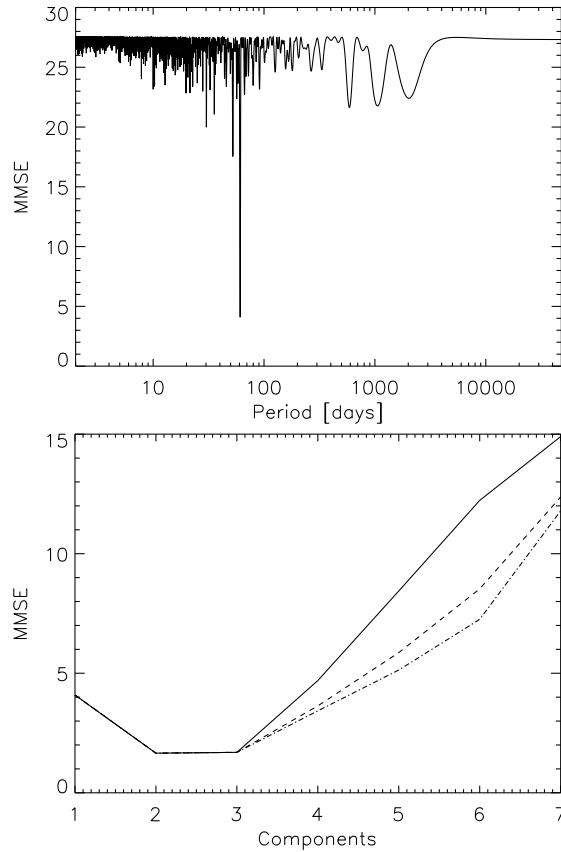


Figure 8. The top panel shows the MMSE periodogram for the full GJ876 data set from Keck. The lower panel shows the results from the Trellis component analysis. The three neighbourhood widths were 11 (solid curve), 13 (dashed curve), and 15 (dot-dashed curve), meaning within the trellis analysis we chose to include 11, 13, and 15 neighbouring spikes on either side of the frequency spike we are testing.

Fig. 8), for all three neighbourhood widths we chose. This result not only adds weight to the reality of these signals, but also gives us confidence in our analysis procedure, since the component search rules out all other peaks we selected as being simply noise related.

Next, we proceeded to split the data into two chunks of equal length as a function of time and run the analysis again, clearly detecting both peaks in both chunks of data. Again we get the same results from the component search, showing this method is very efficient at sifting through frequencies that are noise related and those that are genuine. We then measured the phases of both signals from both chunks of data, essentially giving four phase measurements, two from the two signals in the first half of the timeseries and two from the two signals in the second half of the timeseries, and compared the difference of these two phases to test if the phase difference between the two signals is stationary as a function of time.

In the top panel in Fig. 9 we show the results of these tests on a phase diagram and we can see that the symbols representing all the timeseries and only the first and second

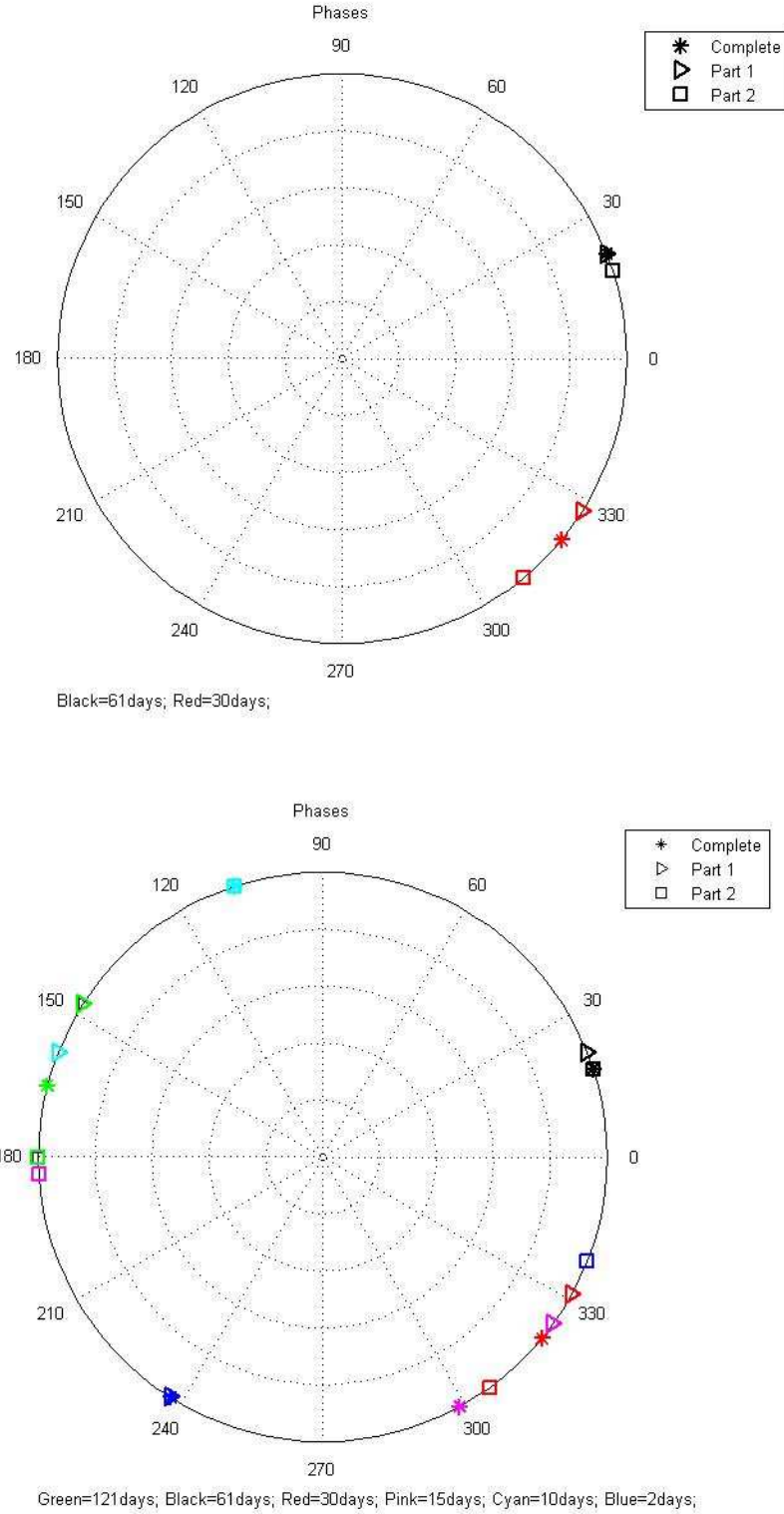


Figure 9. Phase tests for GJ876b and GJ876c are shown in black and red symbols respectively in the top plot, and in the bottom plot for all detected signals. The symbols represent the measured phase of the detected MMSE signals for the complete timeseries (asterisks), the first half of the data set (open triangle), and the second half of the data set (open square). The 360° phase angles are represented on a circular phase plot, with the symbols plotted at the extremum of the plot. A key is also included in the top right that explains the symbols. The colours of the symbols for all signals in the bottom panel are labeled as follows: 61 days (Black), 30 days (Red), 15 days (Pink), 2 days (Blue), 10 days (Cyan), and 121 days (Green)

halves of the timeseries all have similar phase values, and hence the phase offset between both the planets does not change as a function of time. This adds weight to the reality of the planetary system, showing that the signals are stable over the time baseline of the data set, expected from a true Doppler signal induced by an orbiting companion. Therefore, our method allows secondary tests that can be used to confirm the reality of long-baseline data, and a similar analysis can be performed using the amplitudes of the signals, as these should also be stationary with time for a real Doppler signal. A caveat to the method is that for signals that appear weak in the MMSE analysis, which in this case is the 30 day signal in the two halves of the data, the frequency sampling must be increased to ensure one selects the proper frequency peak to test. This is because in the local neighbourhood of frequency peaks surrounding a genuine signal peak, the frequencies and amplitudes vary very little but the phase varies a lot, and hence one must be sure to select the correct peak originating from the genuine Doppler signal.

This test shows that our MMSE method allows us to confirm the nature of signals as 1) being real signals present in the data, and 2) being signals that are stable in phase as a function of time, increasing the likelihood that they are real Doppler signals and not quasi-static signals originating from time-varying phenomena. The caveat here is that the signals being tested must be significant in both halves of the timeseries so that one can select them unambiguously in the data. This analysis can also be performed using the signal amplitudes and frequencies. These features of our MMSE method present a step beyond single LSP-like methods, as additional information is extracted from the data in the processing of the periodogram.

Finally, since we believe the phase analysis can be used as a robust way to determine if signals are planets or not, we apply it to the rest of the sample to test if the other signals we detect conserve their phase. The lower plot in Fig. 9 shows the phases calculated as before but including the additional four signals. We note that the other signals are not as significant as the first two but we believe we can select the correct frequency spike from both halves of the data series.

The most significant of the additional four signals is the 15 day signal and as it is in the next resonant site for a real planet, there is an additional reason to believe it could be real. We show the measured phases in pink in the figure and we find that the complete data and the first half data are in good agreement, however the second half of the data shows a phase that is around 120 degrees away from the complete data, throwing doubt on the nature of

Table 1. Keck and HARPS-TERRA radial velocities for GJ876.

JD days	RV m/s	Error m/s
<u>Keck</u>		
602.09311	329.19	2.68
603.10836	345.30	2.70
604.11807	335.99	2.77
605.11010	336.00	2.78
606.11129	313.94	2.75
607.08450	288.73	2.75
609.11637	197.05	2.81
666.05032	338.38	2.68
690.00713	-115.22	2.87
715.96471	197.16	2.63
785.70436	365.44	3.39
983.04582	-65.63	2.74
984.09389	-84.80	2.83
1010.04457	-43.58	2.60
1011.10207	-26.76	2.38
1011.98546	-0.63	2.28
1013.08905	26.92	2.70
1013.96558	50.29	2.41
1043.02045	-45.34	2.66
1044.00022	-70.50	2.67
1050.92784	-115.86	2.72
1052.00302	-98.84	2.89
1068.87655	-90.26	2.75
1069.98405	-61.21	2.79
1070.96594	-56.96	2.81
1071.87782	-27.61	2.73
1072.93848	-16.71	2.70
1170.70376	-86.04	3.12
1171.69171	-99.71	2.89
1172.70252	-81.15	2.84
1173.70148	-78.61	2.94
1312.12727	-103.43	2.69
1313.11723	-101.40	2.69
1343.04074	68.57	2.80
1368.00106	-147.61	2.84
1369.00183	-156.59	2.89
1370.05951	-139.31	2.61
1372.05858	-120.61	3.54
1409.98670	-49.88	2.75
1410.94861	-48.68	2.81
1411.92171	-56.68	2.66
1438.80200	-23.37	2.84
1543.70165	-105.40	2.96
1550.70152	-161.29	2.77
1704.10273	157.72	2.68
1706.10773	107.70	2.86
1755.98025	307.51	3.26
1757.03786	281.33	2.94
1792.82213	-179.43	2.79
1883.72512	226.87	2.74
1897.68199	88.28	2.83
1898.70648	80.85	2.82
1899.72426	70.86	2.77
1900.70359	51.60	2.65
2063.09867	245.77	2.93
2095.02441	-194.59	2.95
2098.05057	-230.27	3.09
2099.09480	-222.44	3.08
2100.06624	-234.09	2.70
2101.99145	-214.27	2.77
2128.91479	167.27	3.11
2133.01847	92.78	3.00
2133.88182	105.82	3.16

2160.89624	-226.42	2.81
2161.86235	-231.15	3.03
2162.88042	-195.02	3.11
2188.90903	156.83	2.84
2189.80815	152.59	3.16
2236.69389	225.13	2.81
2238.69635	248.60	2.92
2242.71316	264.24	3.16
2446.07064	117.43	3.19
2486.91681	230.06	2.54
2487.12395	218.81	2.47
2487.91836	216.56	2.60
2488.12695	222.24	2.48
2488.94388	199.66	2.19
2514.86655	-84.38	3.19
2515.87295	-108.41	3.00
2535.77402	83.48	3.05
2536.02384	87.44	2.87
2536.80403	114.45	3.03
2537.01292	117.70	2.76
2537.81194	126.07	2.80
2538.01383	133.42	3.00
2538.80067	162.08	3.07
2539.92124	175.89	2.79
2572.71250	-7.07	2.67
2572.91949	-15.40	2.77
2573.74296	-28.24	2.65
2573.87844	-28.58	2.62
2574.76393	-66.20	2.61
2574.94041	-64.63	2.67
2575.71905	-87.17	2.56
2600.75110	172.51	2.42
2601.75071	177.92	2.48
2602.72004	201.51	2.52
2651.71796	-78.56	3.91
2807.02778	202.50	2.79
2829.00786	-205.85	2.81
2832.07993	-137.56	2.95
2833.96325	-87.32	2.91
2835.08493	-51.90	2.74
2848.99946	188.48	3.25
2850.00090	171.94	3.01
2851.05668	166.92	3.10
2854.00713	130.49	2.92
2856.01579	155.93	3.00
2897.82598	-2.50	2.87
2898.81468	29.81	2.88
2924.79475	255.62	3.03
2987.71613	246.15	3.58
2988.72395	239.18	3.07
3154.11700	95.22	3.00
3181.00540	-14.91	3.00
3181.11618	-22.60	2.90
3182.06964	-60.62	2.79
3191.03662	-220.60	2.94
3195.97023	-140.86	2.94
3196.99712	-122.80	3.11
3301.83459	13.71	2.37
3302.72877	-36.34	2.31
3303.78576	-85.95	2.36
3338.74360	119.33	2.91
3367.71753	-180.10	3.12
3368.71947	-193.13	3.31
3369.70562	-192.62	2.54
3547.08770	-98.83	2.64
3550.10132	-148.44	2.99
3551.10883	-166.49	2.94

3552.09458	-165.40	2.89
3571.00432	27.08	2.86
3603.07412	104.97	3.19
3604.01707	51.89	2.93
3604.98440	13.84	3.16
3724.71853	88.50	2.80
4083.77192	287.58	3.28
4337.09682	-0.28	2.99
4343.91291	-109.95	3.10
4345.11351	-93.51	2.96
4396.78303	27.97	2.88
4397.84797	-4.46	2.99
4634.10109	182.38	2.94
4636.08653	132.28	2.91
4639.07368	64.12	2.79
4667.05860	-137.50	2.8
4672.99139	-31.83	2.54
4675.95043	73.06	2.45
4687.00220	318.88	2.80
4702.07311	9.81	2.64
4703.06794	-0.30	2.29
4704.02881	-25.07	2.53
4819.80176	99.74	2.68
4822.78895	25.41	2.51
5051.08321	284.20	2.56
5054.03189	274.77	3.01
5143.87496	-127.21	2.39
5166.83669	250.15	2.41
5168.79585	272.52	2.58
5200.76205	-59.18	2.52
5201.76137	-78.29	2.42
5202.73775	-103.93	2.28

HARPS

3339.55769	210.90	2.18
3542.76959	175.44	2.19
3542.93864	162.55	2.10
3543.75050	112.82	2.09
3543.87080	108.38	2.07
3543.94632	106.84	2.09
3544.74647	72.35	2.17
3544.87437	67.05	2.06
3544.94455	63.42	2.08
3545.78504	28.25	2.66
3546.73885	0.00	2.58
3546.88000	-7.65	2.06
3546.94738	-10.10	2.14
3547.73491	-33.05	2.32
3547.86712	-35.70	2.07
3547.94555	-34.82	2.13
3550.73512	-76.60	2.18
3550.84190	-79.72	2.08
3550.94392	-83.54	2.11
3572.85339	89.75	2.25
3573.77291	87.62	2.09
3576.74516	87.28	2.06
3577.71674	109.28	2.06
3577.89513	109.51	2.07
3579.86570	149.02	2.06
3669.66480	-33.22	2.10
3670.50887	-38.22	2.08
3670.71111	-43.30	2.09
3671.50963	-63.62	2.07
3671.71358	-63.10	2.12
3672.51327	-64.64	2.05
3672.70490	-70.00	2.07

3673.51828	-84.75	2.10
3673.70526	-83.97	2.07
3674.50616	-81.30	2.05
3674.69603	-87.32	2.10
3675.51016	-95.90	2.09
3975.72341	-29.59	2.06
3979.81110	-64.72	2.19
4228.89045	22.46	2.09
4260.93227	463.58	2.35
4291.86547	29.54	2.13
4295.79232	-25.12	2.04
4298.80154	-44.60	2.09
4339.71897	18.95	2.07
4344.75827	-14.39	2.07
4392.62420	206.68	2.08
4422.54302	-40.55	2.14
4429.56649	66.48	2.11
4446.56696	372.04	2.08
4704.71839	48.06	2.08
4770.68394	94.21	2.14

Table 2. Keplerian solutions for GJ876.

Parameter	GJ876 <i>b</i>	GJ876 <i>c</i>	GJ876 <i>d</i> *	GJ876 <i>e</i>	GJ876 <i>f</i> *	GJ876 <i>g</i>
<i>P</i> [days]	61.03±3.81	30.23±0.19	15.04±0.04	1.94±0.001	10.01±0.02	124.69±90.04
<i>e</i>	0.000±1×10 ⁻³	0.002±1×10 ⁻³	0.007±0.004	0.081±0.040	0.090±0.046	0.073±0.048
ω [°]	116.7±1.1	225.2±5.0	78.3±10.3	157.4±23.3	88.0±10.5	360.0±15.8
<i>M</i> ₀ [°]	259.5±1.1	117.9±5.0	198.5±10.4	79.9±23.7	108.3±10.5	230.2±16.3
<i>K</i> [ms ⁻¹]	211.57±32.92	88.72±13.81	20.71±3.24	5.91±0.98	5.00±0.80	3.37±0.53
<i>m_p sin i</i> [M _J]	1.927±0.003	0.637±0.002	0.118±0.002	0.017±0.001	0.025±0.001	0.039±0.001
γ_{Keck} [ms ⁻¹]	-49.68±0.50					
$\gamma_{\text{HARPS-TERRA}}$ [ms ⁻¹]	-79.23±0.63					
σ_J [ms ⁻¹]	1.98±					
rms [ms ⁻¹]	3.33					
χ^2	1.787					

Table 3. * Assumes the signal relates to a Doppler shift induced by an orbiting planet.

the signal. However, it must be remembered that this would be the smallest of the three gas giant planets in the resonance.

When we look at the other signals in this manner we note that the planet at ~ 2 days shows some phase variations at a similar level to that of the 15 day signal. Again, the amplitude of this signal is even lower than the previous ones so its significance is lower and makes it difficult to select the correct spikes in the analysis in half of the data. The phase of the signal at 10 days shows some variation, albeit at a lower level than the 2 and 15 days signals, whereas the 124 day planetary signal clearly conserves the phase in both halves of the data, helping to confirm it's reality as a Doppler signal.

Although the 2, 15, and 10 day signals exhibit some phase variation with time, at least some of this could be due to the dynamical nature of the system, especially the Laplace resonance. However, we also note that if we just include the three signals with periods of 61, 30, and 2 days, we find the phase to be more stable for the 2 day planetary signal. Therefore,

it could be that including signals that are not stable Doppler signals induces phase variations on other stable signals. Also it could be the case that the 2 and 15 day signals are correlated at some level, meaning when we analyse them both in parallel the correlations manifest as phase variations in the timeseries.

6 SUMMARY AND FUTURE WORK

We have developed and tested a new method for detecting and analysing possible signals in unevenly sampled timeseries data, with a particular emphasis on the analysis of precision radial velocities to search for low-mass exoplanets. Our method begins with a new periodogram like analysis of the data, using a minimum mean squared error approach that allows us to determine the amplitude and phase of the possible signal directly. We then select the periodogram spikes we want to analyse and make use of a trellis-type analysis to test which of these peaks are related to real signals and which are noise spikes attributed to interference from the window function. Our method is a global approach that hunts for all signals in the full data set, given by the distribution of frequency spikes measured in the data. The trellis analysis is a generic solution that is only limited in scope by the available computing power. Finally, we can monitor the amplitudes and phases as a function of time to test if the signals we have found are stationary signals, like those from a Doppler source, or if they are non-stationary, arising from aliases or from external quasi-stationary sources like spot modulated activity on the star.

The following seven points summarise the benefits of our MMSE approach:

- (i) The MMSE method offers a unified framework to estimate the optimum number of components, and their parameters, in an unevenly sampled data set.
- (ii) The MMSE approach attempts to estimate the global optimal solution (i.e. number of components, their frequencies, amplitudes, and phases) by using an analysis based on a simultaneous set of components and eliminating the dependence on the order in which the strongest frequencies are selected.
- (iii) The model behind the MMSE method is more complete than standard periodogram approaches since it takes into consideration that the uneven sampling distortion depends on all the true components in the observed signal.
- (iv) The MMSE approach is not an iterative process and no subjective stop criterion is required. However, a gradient-based approach can be performed without considering the

trellis component search part of the process, allowing a direct comparison of results gained from a LSP-like analysis.

- (v) No information about the window function is required.
- (vi) The MMSE is robust against false-positives and false-negatives.
- (vii) The MMSE method is also a powerful and generic tool to validate Doppler-like signals found by other methods.

We applied our method to the Keck and HARPS data for the M-dwarf planet host star GJ876, known to host a system of planets that contains at least two short period gas giants. We studied this system because the large amplitude signals could be detected in both halves of the timeseries separately. This allowed us to study the phase of the signal as a function of time, showing that the phase difference between both planets is stable over the length of the timeseries and therefore adding weight to the reality of these signals. This analysis shows the power of our method over the LSP, since this gives no information on the signal parameters except for the frequency.

Further to this, we find an additional two planet-like signals in the data, having periods of 10 and 15 days, the latter of which could contain islands of stability linked by a 8:4:2:1 chain resonance. However, given previous Newtonian integrational methods failed to spot these strong signals, we require further dynamical analyses to confirm if such a planetary configuration is stable over the long-term. Indeed, we find phase variations with time for both of these signals, along with the signal at 2 days also, which could throw doubt on the origin of these signals as being from orbiting planets. However since the signals are weak, this analysis is as yet inconclusive.

Finally, we plan to continue building our analysis algorithm, in particular working on a better understanding of the noise. We aim to add a red noise model component that will allow us to better deal with correlations in the noise and between the data points, likely using a moving average model that has recently been shown to deal well with short term correlations between precision radial velocities (Tuomi et al. 2013; Anglada-Escudé et al. 2013; Jenkins et al. 2013).

ACKNOWLEDGMENTS

We thank our referee Artie Hatzes for a very thorough review of our work. We acknowledge useful discussion with Hugh Jones and Mikko Tuomi. Jenkins acknowledges funding

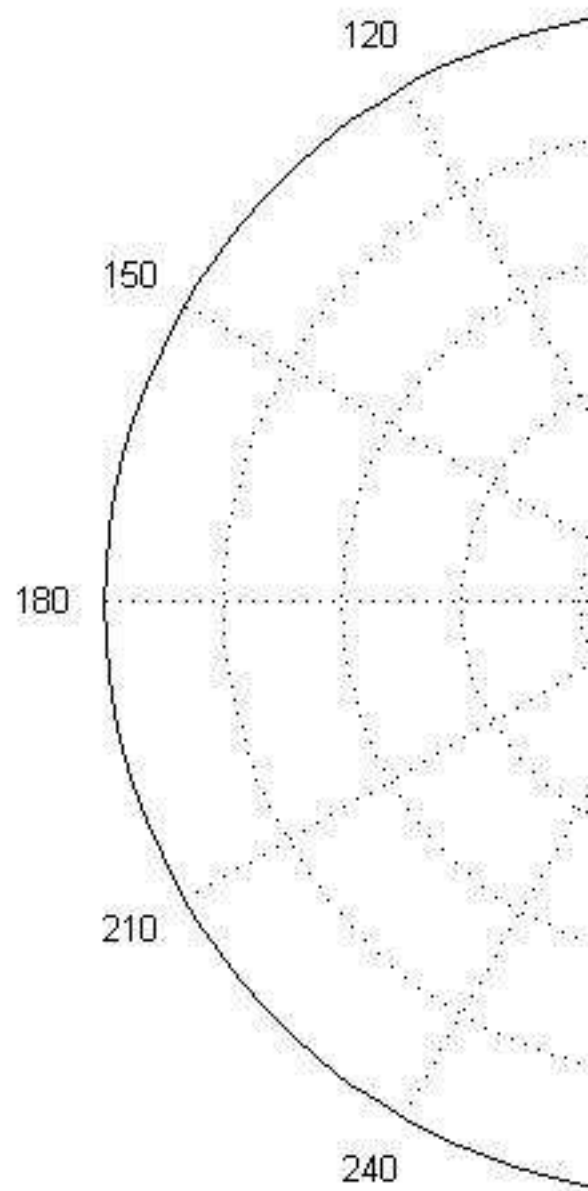
by Fondecyt through grant 3110004, partial support from Centro de Astrofísica FONDAP 15010003, the GEMINI-CONICYT FUND, from the Comité Mixto ESO-GOBIERNO DE CHILE, and from the Basal-CATA grant. Yoma, Rojo, Mahu, and Wuth acknowledge the support of the Conicyt Team Research in Science and Technology Project ACT1120. Rojo also acknowledges support by Fondecyt through grant 1120299.

REFERENCES

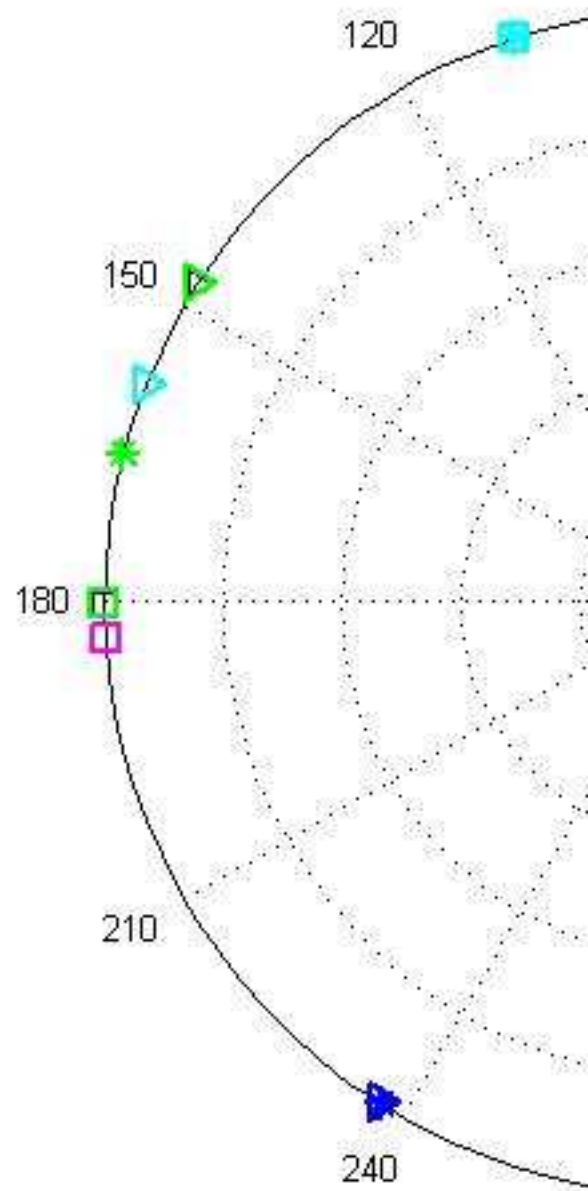
- Anglada-Escudé G., Arriagada P., Vogt S. S., et al. 2012, ArXiv e-prints
- Anglada-Escudé G., Butler R. P., 2012, *ApJS*, 200, 15
- Anglada-Escudé G., López-Morales M., Chambers J. E., 2010, *ApJ*, 709, 168
- Anglada-Escudé G., Tuomi M., 2012, *A&A*, 548, A58
- Anglada-Escudé G., Tuomi M., Gerlach E., Barnes R., Heller R., Jenkins J. S., Wende S., Vogt S. S., Butler R. P., Reiniers A., Jones H. R. A., 2013, *A&A*, 556, A126
- Baluev R. V., 2013, *MNRAS*, 429, 2052
- Bonfils X., Delfosse X., Udry S., Forveille T., Mayor M., Perrier C., Bouchy F., Gillon M., Lovis C., Pepe F., Queloz D., Santos N. C., Ségransan D., Bertaux J.-L., 2013, *A&A*, 549, A109
- Correia A. C. M., Couetdic J., Laskar J., Bonfils X., Mayor M., Bertaux J.-L., Bouchy F., Delfosse X., Forveille T., Lovis C., Pepe F., Perrier C., Queloz D., Udry S., 2010, *A&A*, 511, A21
- Cumming A., 2004, *MNRAS*, 354, 1165
- Dawson R. I., Fabrycky D. C., 2010, *ApJ*, 722, 937
- Delfosse X., Forveille T., Perrier C., Mayor M., 1998, *A&A*, 331, 581
- Gerlach E., Haghighipour N., 2012, *Celestial Mechanics and Dynamical Astronomy*, 113, 35
- Hatzes A. P., 2013, *ApJ*, 770, 133
- Hatzes A. P., Dvorak R., Wuchterl G., Guterman P., Hartmann M., Fridlund M., Gandolfi D., Guenther E., Pätzold M., 2010, *A&A*, 520, A93
- Jenkins J. S., Jones H. R. A., Goździewski K., Migaszewski C., Barnes J. R., Jones M. I., Rojo P., Pinfield D. J., Day-Jones A. C., Hoyer S., 2009, *MNRAS*, 398, 911
- Jenkins J. S., Jones H. R. A., Tuomi M., Murgas F., Hoyer S., Jones M. I., Barnes J. R., Pavlenko Y. V., Ivanyuk O., Rojo P., Jordán A., Day-Jones A. C., Ruiz M. T., Pinfield

- D. J., 2013, *ApJ*, 766, 67
- Jenkins J. S., Murgas F., Rojo P., Jones H. R. A., Day-Jones A. C., Jones M. I., Clarke J. R. A., Ruiz M. T., Pinfield D. J., 2011, *A&A*, 531, A8
- Jenkins J. S., Tuomi M., Brasser R., Ivanyuk O., Murgas F., 2013, *ApJ*, 771, 41
- Kuschnig R., Weiss W. W., Gruber R., Bely P. Y., Jenkner H., 1997, *A&A*, 328, 544
- Lenz P., Breger M., 2004, in Zverko J., Ziznovsky J., Adelman S. J., Weiss W. W., eds, *The A-Star Puzzle Vol. 224 of IAU Symposium, Period04: A software package to extract multiple frequencies from real data.* pp 786–790
- Marcy G. W., Butler R. P., Fischer D., Vogt S. S., Lissauer J. J., Rivera E. J., 2001, *ApJ*, 556, 296
- Mayor M., Bonfils X., Forveille T., Delfosse X., Udry S., Bertaux J.-L., Beust H., Bouchy F., Lovis C., Pepe F., Perrier C., Queloz D., Santos N. C., 2009, *A&A*, 507, 487
- Meschiari S., Wolf A. S., Rivera E., Laughlin G., Vogt S., Butler P., 2009, *PASP*, 121, 1016
- Morbidelli A., Levison H. F., Tsiganis K., Gomes R., 2005, *Nature*, 435, 462
- O’Toole S. J., Tinney C. G., Jones H. R. A., Butler R. P., Marcy G. W., Carter B., Bailey J., 2009, *MNRAS*, 392, 641
- Queloz D., Bouchy F., Moutou C., et al. 2009, *A&A*, 506, 303
- Rivera E. J., Butler R. P., Vogt S. S., Laughlin G., Henry G. W., Meschiari S., 2010, *ApJ*, 708, 1492
- Rivera E. J., Lissauer J. J., Butler R. P., Marcy G. W., Vogt S. S., Fischer D. A., Brown T. M., Laughlin G., Henry G. W., 2005, *ApJ*, 634, 625
- Scargle J. D., 1982, *ApJ*, 263, 835
- Tsiganis K., Gomes R., Morbidelli A., Levison H. F., 2005, *Nature*, 435, 459
- Tuomi M., 2012, *A&A*, 543, A52
- Tuomi M., Jenkins J. S., 2012, *ArXiv e-prints*
- Tuomi M., Jones H. R. A., Jenkins J. S., Tinney C. G., Butler R. P., Vogt S. S., Barnes J. R., Wittenmyer R. A., O’Toole S., Horner J., Bailey J., Carter B. D., Wright D. J., Salter G. S., Pinfield D., 2013, *A&A*, 551, A79
- Vogt S. S., Butler R. P., Rivera E. J., Haghighipour N., Henry G. W., Williamson M. H., 2010, *ApJ*, 723, 954
- Wittenmyer R. A., Horner J., Tuomi M., Salter G. S., Tinney C. G., Butler R. P., Jones H. R. A., O’Toole S. J., Bailey J., Carter B. D., Jenkins J. S., Zhang Z., Vogt S. S., Rivera E. J., 2012, *ApJ*, 753, 169

Zechmeister M., Kürster M., 2009, A&A, 496, 577



Black=61 days; Red=30 days;



Green=121days; Black=61days